Journal of Power Sources 212 (2012) 86–92

Contents lists available at SciVerse ScienceDirect

Journal of Power Sources

journal homepage: www.elsevier.com/locate/jpowsour

A reduced temperature solid oxide fuel cell with three-dimensionally ordered macroporous cathode

Bo Liang [a,*], Toshio Suzuki [a], Koichi Hamamoto [a], Toshiaki Yamaguchi [a], Hirofumi Sumi [a], Yoshinobu Fujishiro [a], Brian J. Ingram [b], John David Carter [b]

[a] National Institute of Advanced Industrial Science and Technology, Shimo-shidami, Moriyama-ku, Nagoya 463-8560, Japan
[b] Argonne National Laboratory, Argonne, IL, USA

ARTICLE INFO

Article history:
Received 27 February 2012
Received in revised form
27 March 2012
Accepted 30 March 2012
Available online 13 April 2012

Keywords:
Micro tubular
Solid oxide fuel cell
Macroporous cathode
Triple-phase boundary

ABSTRACT

Three-dimensionally ordered macroporous cathode was fabricated for a zirconia based micro-tubular solid oxide fuel cells (SOFCs). Three different cathodes (cathode A, no pore former; cathode B, with pore former (1.5 μm in diameter); cathode C, with pore former (0.8 μm in diameter)) were compared to investigate how the microstructure of it affected the cell performance at various operating temperatures. Micro-sized pores were well distributed within cathode B and C. The total porosity of cathode A is 35%, while it respectively reached 42 and 50% for cathodes B and C. At the same time, the specific surface area of them was 28.8 and 52.0% larger than that of the cathode A. As a result, the peak power density of the zirconia based cell, with cathode C, was 0.25 and 0.56 W cm^{-2} at 550 and 600 °C, while the respective value was just 0.11 and 0.30 W cm^{-2} for the cell with cathode A. Thus, optimizing microstructure of cathode should be one of the best approaches for lowering the operating temperature for SOFCs.

1. Introduction

High temperature operating of SOFCs limits the selection of materials for the cells, module components, as well as their use for quick strat-up operation [1–4]. Thus, many studies of SOFCs aim at lowering the operating temperature. In recent years, significant effort has been devoted to the research for new electrodes and electrolyte. For examples, $La_{0.9}Sr_{0.1}Ga_{0.8}Mg_{0.2}O_{3-\delta}$ (LSGM), as SOFCs electrolyte (2 μm thick), has been shown to achieve peak power density of 2 W cm^{-2} at 600 °C [5]. Ba-based and $LaCrO_3$-based perovskite-type oxide were effective to be respectively used as cathode and anode materials. $Ba_{0.5}Sr_{0.5}Co_{0.8}Fe_{0.2}O_{3-\delta}$ (BSCF), incorporated into a thin-film doped ceria fuel cell, exhibits high power densities of 1.01 W cm^{-2} at 600 °C [6]. $La_{0.75}Sr_{0.25}Cr_{0.5}Mn_{0.5}O_3$ (LSCM) was reported as nickel-free anode material, with comparable electrochemical performance to Ni/YSZ cermets [7]. $Ba(Zr_{0.1}Ce_{0.7}Y_{0.2})O_{3-\delta}$ at temperatures below 550 °C, displays very high ionic conductivity of all known electrolyte materials for proton conducted SOFC applications [8]. A thin and highly-textured $BaZr_{0.8}Y_{0.2}O_{3-\delta}$ film even shows applicable proton conductivity at 350 °C for micro-fabricated SOFC devices [9]. Other approaches for low temperature operation of SOFCs included to optimize the anode microstructure and to decrease thickness of the electrolyte. a power density as high as 0.4 W cm^{-2} at 400 °C was demonstrated using 100 nm-thick zirconia based electrolyte [10]. Macroporous anode supported SOFCs had a power density of greater than 1 W cm^{-2} at 600 °C with conventional SOFCs materials [11].

Besides that, surface-decoration of perovskites on electrodes were also introduced to SOFCs to achieve high performance. "Sr"-decoration with nanoparticle coverage in the range from 50% to 80% of the $La_{0.8}Sr_{0.2}CoO_{3-\delta}$ (LSC) surface enhanced the surface exchange coefficient by an order of magnitude [12]. A pure-ceria (CeO_2) functional layer on the surface of anode enhanced the tubular cell performance below 500 °C using methane-water mixture fuel [13]. Also, several articles were reported in highly porous cathodes with optimized microstructure [14–17]. They showed an increasing cell performance at relatively high operating temperatures (650–900 °C). Fox example, yttriastabilized zirconia (YSZ) nanofiber scaffold with the infiltrated $La_{1-x}Sr_xMnO_3$ (LSM), as cell cathode, had an enhanced catalytic activity for oxygen reduction and an increased number of triple-phase boundary sites.

In this study, three different macroporous cathodes were systematically investigated to lowering the operating temperature of SOFCs, of which included total porosity, specific surface area, pore volume, exchange current density, cathode conductivity and

* Corresponding author. Tel.: +81 52 736 7581; fax: +81 52 736 7405.
E-mail addresses: basafan@gmail.com, boliang-riyou@aist.go.jp (B. Liang).

0378-7753/$ – see front matter © 2012 Elsevier B.V. All rights reserved.
doi:10.1016/j.jpowsour.2012.03.107

Table 1
The particles size used in anode-electrolyte.

	ScSZ	YSZ	GDC	NiO	PMMA(anode)	PMMA(cell B)	PMMA(cell C)
D50 (μm)	0.62	0.022	0.63	0.1	5	1.5	0.8

IV performance. The micro-tubular design was used, which can realize a high volumetric power density and endure thermal stress cause by rapid heating up or cooling down [18–23]. $La_{0.6}Sr_{0.4}Co_{0.2}Fe_{0.8}O_{3-\delta}$ (LSCF) was selected as cathode material due to its excellent ionic-electronic conductivity and high activity for the oxygen reduction reaction [24–26].

2. Experimental section

Anode tubes were made by mixing of NiO powder, YSZ, 40 vol% of pore former (poly methyl methacrylate (PMMA) beads (5 μm in diameter)), and binder (cellulose base). These powders were mixed for 1 h by a mixer, 5DMV-r. After adding proper amount of water, it was stirred for 30 min in a vacuum chamber. The mixture (clay) was aged for 15 h. Then, anode tubes were extruded from a metal mold by using a piston cylinder type extruder (Ishikawa-Toki Tekko-sho Co., Ltd.). Using co-sintering process, a very thin scandium stabilized zirconia (ScSZ) (Daiichiki-genso Co., Ltd.) electrolyte about 5 μm was securely fabricated on the anode tubes. In detail, the anode tubes were dipped in ScSZ slurry and coated at a pulling rate of 1 mm s^{-1}. The slurry consisted of ScSZ powder, binder (polyvinyl butyral) as well as solvents (toluene and ethanol). The coated film on anode tube was dried, then, the anode-electrolyte were co-sintered 1350 °C for 1 h in the air. They were again dip-coated using GDC slurry and sintered at 1200 °C. The cell was co-sintered at 1350 °C.

Next, the anode tubes with an electrolyte (ScSZ) and interlayer (GDC) were dip-coated in a cathode slurry. In this study, three different cathodes were prepared, corresponding to with and without pore former: cathode A (no PMMA used), cathode B (PMMA beads, 1.5 μm in diameter), and cathode C (PMMA beads, 0.8 μm in diameter). All the cathodes have same anode support and electrolyte, as well as interlayer. The slurry of cathode A consisted of LSCF, GDC powders (weight ratio to LSCF is 3:1) as well as organic ingredients (toluene and ethanol). As for the slurries of cathodes B and C, the weight ratios of pore former/(LSCF, GDC) powder were different. In order to avoid cracks during sintering process, they were 1/6.6 (for 0.8 μm PMMA beads) and 1/13.2 (for 1.5 μm PMMA beads). After dip-coating the cathode slurry, the tubes were dried and sintered at 1050 °C for 1 h in the air to complete a cell. Also, the cell A, cell B, and cell C respectively corresponded with the cell with cathode A, cathode B, and cathode C.

Table 1 provides the size of particles/beads used in the cells. D50 is particle diameter value in case cumulative distribution percentage reaches 50%.

The cathode surface area and porosity were measured by mercury porosimeter. The fabrication method of bulk cathode (cathode A, B, and C) is multi times dip-coating (repeated the dip-coating after dry) on a ceramic tube (5 mm in diameter). The lifting speed of ceramic tube from cathode slurry is 2 mm s^{-1}, which is exactly same to the speed in fabricating cathode layer on a cell. The microstructure of the tubular cell was observed by using SEM (JEOL, JSM 6330F). Open circuit voltage, I–V plots, and electrochemical impedance spectroscopy (EIS) plots were collected using a multi-channel potentiostat (Solartron 1260 frequency response analyzer with a 1296 Interface). Ag wires were used for collecting current of the anode and cathode sides, which were both fixed by painting a colloidal silver paste. The current collection from the anode side was made from an edge of the anode tube, and the collection from cathode side was made from the whole cathode area. The tubular cell was sealed at an alumina tube using a ceramic sealing paste. Hence, the anode contact was not exposed to air. Dry and diluted hydrogen (20% H_2 + 80% Ar) was flowed inside the tubular cell at a flow rate of 54 mL min^{-1}. The cathode was open to the air without flowing gas. The size of the cell was about 1.85 mm in diameter, 30 mm in tube length. The active cathode area is 0.5–0.6 cm^2. The tubular cells were tested at the temperature of 500, 550, 600, and 650 °C, which were tested by a thermocouple placed closed to the cell.

3. Results and discussion

A pictorial cell (cell C) and the fracture cross-sectional SEM image of the cell are shown in Fig. 1(a) and (b). As can be seen, a macroporous cathode layer (LSCF) was coated on the tube surface, with thickness of 20 μm. The anode-electrolyte was co-sintered at

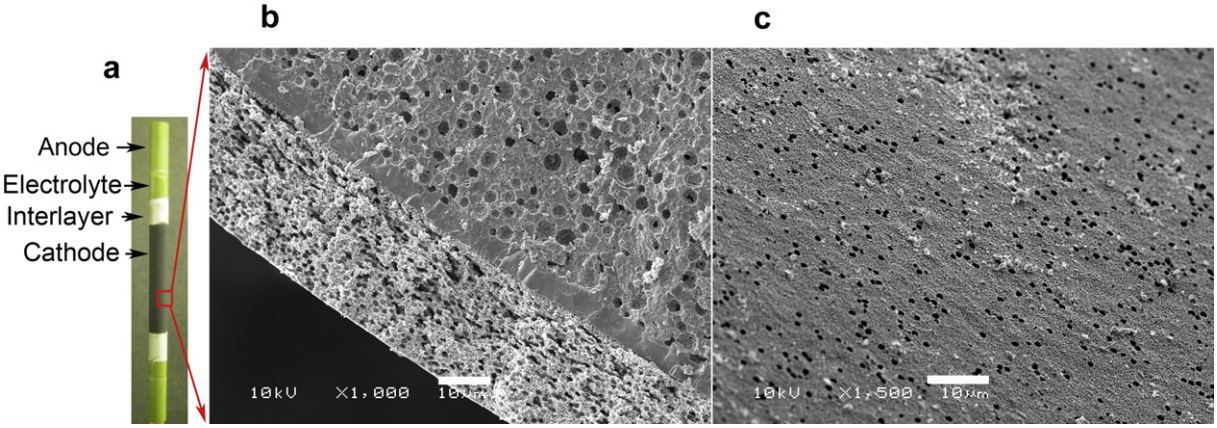

Fig. 1. (a) photography, and (b) Cross-sectional SEM image of a anode supported SOFC with microporous cathode. (c) The surface morphology of LSCF cathode on the cell. The thickness of electrolyte is 5 μm.

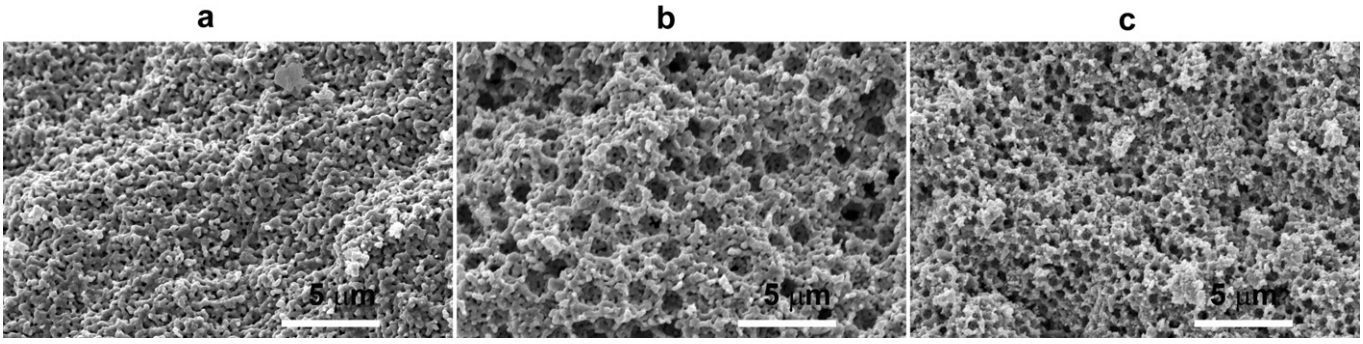

Fig. 2. Microstructure of a macroporous cathode (bulk). (a) without PMMA beads and using PMMA beads as pore former. (b) PMMA beads, 1.5 μm in diameter. (c) PMMA beads, 0.8 μm in diameter. The bulk was prepared by the same method (dip coating with more times) to that of fabricating a cell.

1350 °C. In our previous work [27], 1350 °C prefers to co-sinter a high quality cell. Here, the pore former in cathode burned at around 400 °C and as a result it became pores (round or oblate). The pore formers used in cathodes B and C were in the size of micros and sub micros. At the same time, macro pores were also existed on the cathode surface. As can be seen in Fig. 1(c), the size of pores is almost same to those within cathode. The existence of pores help the oxygen gas transportation.

Fig. 2 show the SEM micrographs of bulk cathodes sintered at 1050 °C. Fig. 2 (b) and (c) respectively corresponded to the cathodes B and C in different magnification. As can be seen, uniform macro pores distributed well within cathode. Also, they were three-dimensionally connected. The average pore sizes of cell C and cell B are 0.8 and 1.5 μm, respectively. They were estimated by measuring more than 100 pores selected from the SEM micrographs.

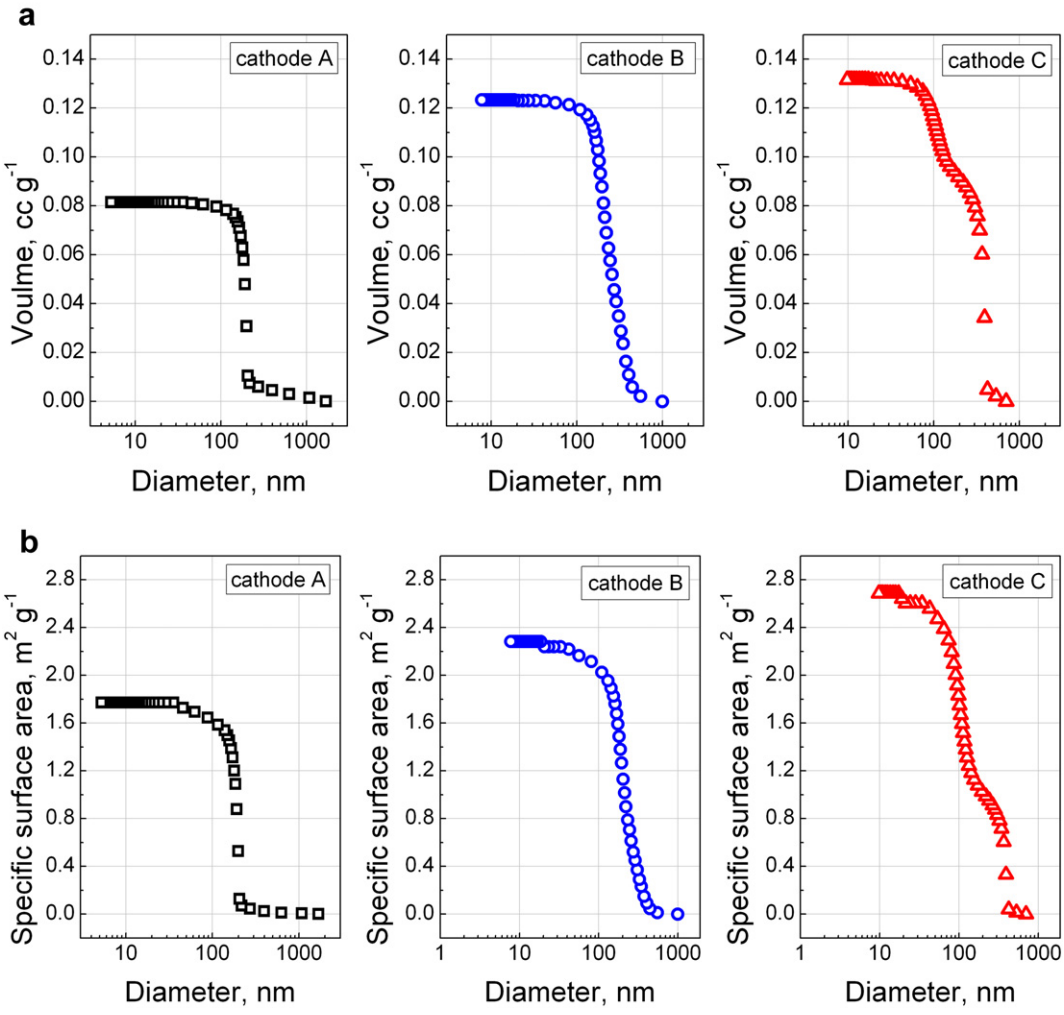

Fig. 3. (a) cumulative pore volume of the three different cathodes. (b) The corresponding specific surface area of the cathodes.

Table 2
Summary of the properties of bulk cathode. The bulk cathode was prepared using dip-coating technology, which is same to the cathode layer for the cells A, B and C.

Cathode samples	Porosity	Specific volume ($cm^3\ g^{-1}$)	Specific surface area ($m^2\ g^{-1}$)
Cathode A	35%	0.08	1.77
Cathode B	42%	0.12	2.28
Cathode C	50%	0.13	2.69

Fig. 3 show the information of cumulative pore volume and specific surface area of different cathodes. As can be seen, the specific surface area of cathode A is just 1.77 $m^2\ g^{-1}$, while it respectively increased 28.8% to 2.28 $m^2\ g^{-1}$ for cathode B and 52.0% to 2.69 $m^2\ g^{-1}$ for cathode C. Large specific surface area of cathode may resulted in large triple-phase boundary (TPB) length, which decrease the polarization loss and improve the electrical performance of cathode.[12] Furthermore, the total pore volume was 0.08, 0.12, 0.13 cc g^{-1} for cathode A, B, and C, respectively. It increased 50 and 62.5% by using pore formers in diameter of 1.5 and 0.8 μm. As a result, the total porosities of cathode A, B, and C were respectively 35, 42, and 50%. Table 2 summarizes the physical properties of each cathode.

Fig. 4 show the performance of the cells A, B and C. In this paper, the effective electrode areas (for calculating power density and exchange current density) were respectively 0.57, 0.56 and 0.59 cm^2 for the cells A, B and C. As can be seen, the peak power density of the cells, with cathodes B and C, were higher than that of cell A at the operating temperatures of 500, 550 and 600 °C. Comparing with cell A, the peak power density of cell C significantly increased 54.4%, 44.3%, and 27.8% to 0.09, 0.25, and 0.56 W cm^{-2} when they operated at 500, 550, 600 °C. Even for the cell B, it still increased 11.6%, 8.9%, and 7.1%. At the same time, the current density of the cell C at 0.7 V (the practical working voltage of a cell) were 0.10, 0.26, 0.5 A cm^{-2}, while it was just 0.06, 0.19, 0.42 A cm^{-2} for cell A. It is noted, as the temperature increased to 650 °C, the peak power density reached about 0.8 W cm^{-2} for all the cells. There was no big difference among them. The cell B even performed slightly worse than the cell A. So, the macroporous structure of cathode showed its advantage at low operating temperatures, and significantly increased the cell performance. When the operating temperature is higher than 650 °C, it was suggested that the anode part maybe become major factor to affect the cell performance, since the cathode structure did not show its influence on the cell performance. It is noted that the improvement of power density is remarkable at relative low operating temperature (500–600 °C). Thus, optimizing microstructure of cathode should be one of the approaches for lowering the operating temperature for SOFCs. Finally, using the macroporous cathode, the peak power density of 0.25 W cm^{-1} (550 °C) and 0.56 W cm^{-1} (600 °C) was successfully achieved for a YSZ bases anode supported cell.

Fig. 5 show the impedance spectra of each cell obtained at various temperatures. They are exactly corresponded to the testing conditions in Fig. 4. As can be seen the high frequency semi-circle of the cell C was clearly observed in Fig. 5 (c) and (d). The value of it was about half of the cell A. It is because the specific surface area of cathode C respectively increased 52.0% comparing with the cathode A. As we knew, large surface area of cathode is considered to be important since it can increase the TPB length. So, the overpotential resistance caused by the electrochemical reaction [13,28] (high frequency semi-circle) of macroporous cathodes became small, especially for cell C. In Fig. 5 (a) and (b), the high frequency and low frequency semi-circles can not be clearly distinguished for the cells

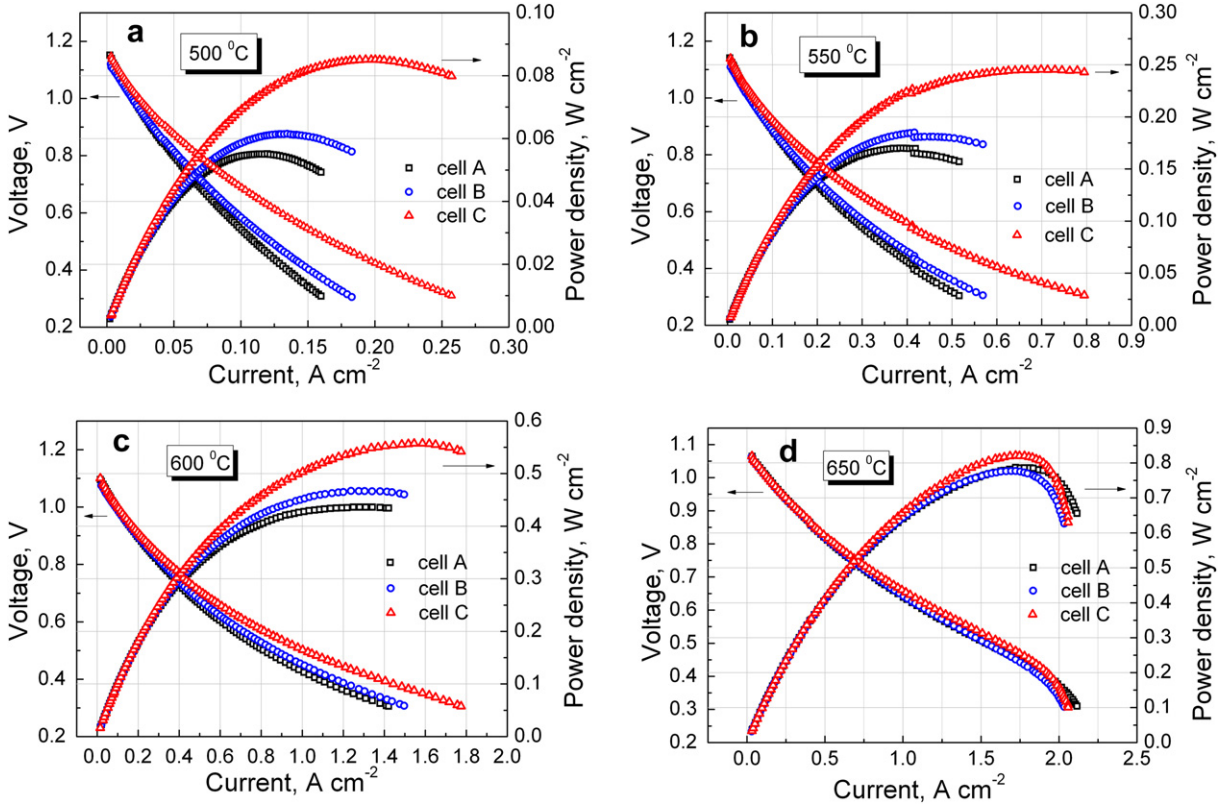

Fig. 4. Performance of the cells. The cell voltage and power density as functions of current at (a) 500 °C, (b) 550 °C, (c) 600 °C and (d) 650 °C.

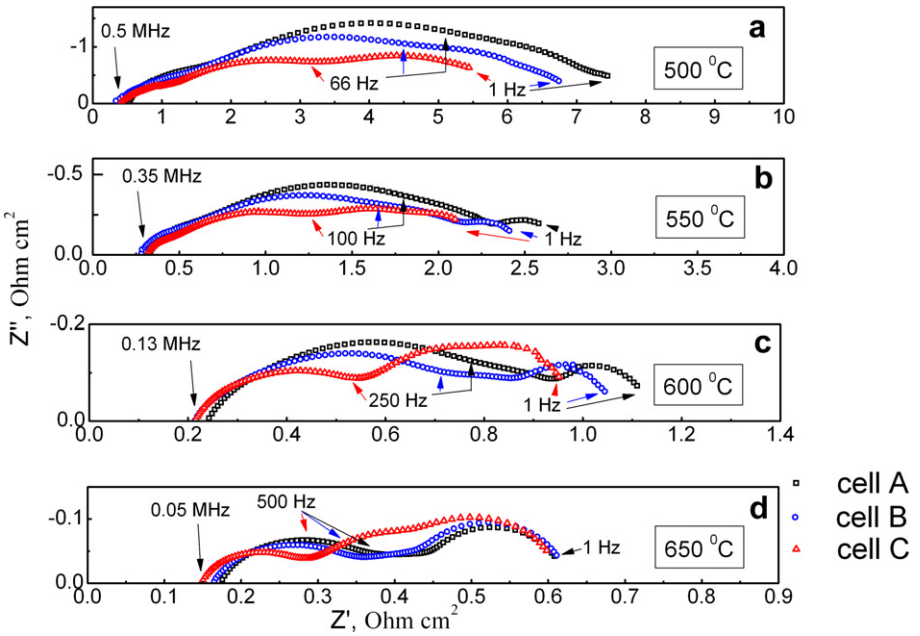

Fig. 5. Impedance spectrum for the cells A, B, and C, which obtained at (a) 500 °C, (b) 550 °C, (c) 600 °C and (d) 650 °C.

A, B and C. However, the plots of the cell C measured at different temperatures showed high frequency semi-circle tend to increase as operating temperature decreased. So, the characteristic frequency of high frequency semi-circle for the cell C was predicted and labeled in Fig. 5(a) and (b). As can be seen, the real over-potential resistance of the cell C caused by electrochemical reaction was still smaller than that of the cells A and B at the same frequency.

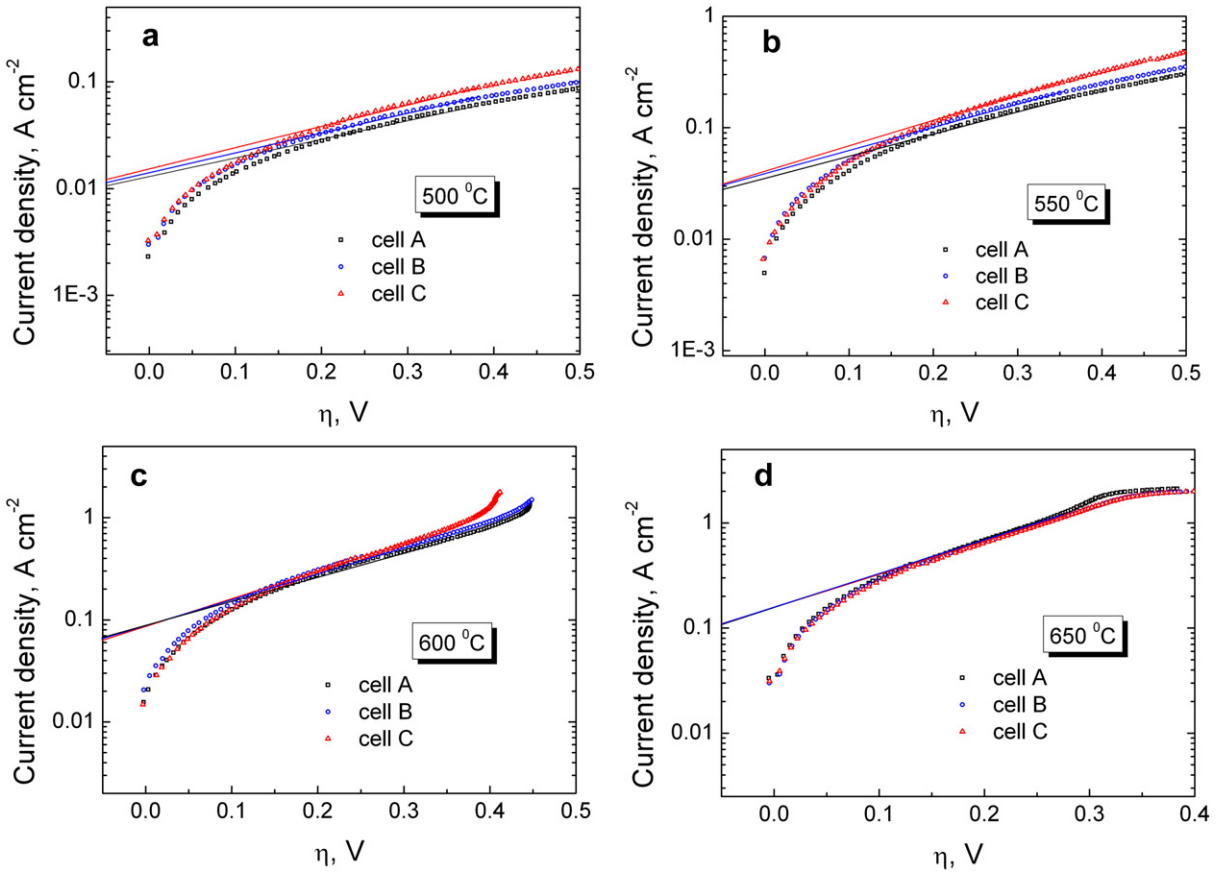

Fig. 6. Tafel plots of the cells measured at various temperature. The cells A, B and C are corresponded to the cathodes A, B and C.

Table 3
Kinetic parameters of cells calculated with curve-fitted parameters for curves shown in Fig. 6. The cells A, B and C are corresponded to the cathodes A, B and C.

Operating temperature	α			j_0 (mA cm^{-2})		
	Cathode A	Cathode B	Cathode C	Cathode A	Cathode B	Cathode C
500 °C	0.15	0.18	0.22	10.0	10.5	11.2
550 °C	0.54	0.59	0.72	28.1	30.1	30.3
600 °C	1.87	2.09	2.53	64	63	61
650 °C	5.74	5.46	5.90	102.2	102.0	101.5

Fig. 6 show the electrode overpotentials of cells obtained by subtracting the ohmic losses for the raw I–V characteristics. All these data follow the following Tafel Eq. (1),

$$\log j = \alpha\eta + \log j_0 \quad (1)$$

where j is the current density, α is transfer coefficient, η is the electrode polarization, and j_0 is the exchange current density. Table 3 tabulates transfer coefficient (α) and the exchange current density (j_0). The value of j_0 was estimated from the Tafel plots in Fig. 6, while the transfer coefficient was calculated with the curve-fitted method in the range of 0.1–0.35 V using the Bulter–Volmer equation. As can be seen, j_0 and α of cell B and cell C is clearly higher than that of cell A at low operating temperatures (500 and 550 °C). Since these cells are exactly same except to the cathode, the difference in the electrode overpotentials is contributed to the difference in the cathode. Compare with cell A, cell C exhibited much lower electrode overpotential especially at high current density. As shown in Fig. 6 (a) and (b), the exchange current density of the cell C is 12.0% and 7.8% higher than that of the cell A, when they were operated at 500 and 550 °C, respectively. It can be explained by the difference of the specific surface area between the cells, which was already shown in Table 2. Furthermore, the transfer coefficient of the cells increased when the macro-sized pores were introduced to their cathode. When the cell operated at 500 °C, it was 0.15 and 0.22 for cell A and cell C, respectively. At 550 °C, the corresponding value for cell A and cell C were 0.54 and 0.79. The increasing of transfer coefficient should be related with the good microstructure and high porosity of cell C. However, less difference even no difference was obtained at relatively high operating temperatures (650 °C), which agrees with the impedance spectrum. In this study, the exchange current of cell C was 30.3 mA cm^{-2} operated at 550 °C, which is comparable to that of YSZ-based cells operated at 800 °C or GDC-based cells operated at 500 °C [29–31].

Because the relative difference of power density among the three types of cells did not coincide with their surface area, the conductivity of them was measured. This shows, from the other side, the inherent drawbacks of the macroporous cathode. As can be seen Fig. 7, the conductivity of cathode B and C is lower than that of cathode A at all testing temperatures, especially for cathode B. The conductivity of cathode A is 85.3 and 81.8 S cm^{-1} at 500 and 600 °C, which is comparable to the value in the literature [32]. Due to the high porosity and microstructure, the respective values of cathode C were 76.1 and 77.5 S cm^{-1} at 500 and 600 °C. As for the cathode B, it decreased sharply to 22.8 and 28.3 S cm^{-1} at corresponding temperatures. The reason possibly was relatively large pores (about 1.5 μm in diameter) in the cathode B lead to make it has less mass density. All in all, the conductivity of cathode C was comparable to cathode A, because the macropore size is relatively small and within sub-micrometer (800 nm). It is noted that the lower conductivity of the porous cathode is tolerated here, because the selection of a micro-tubular design allows an unusual current contact geometry.

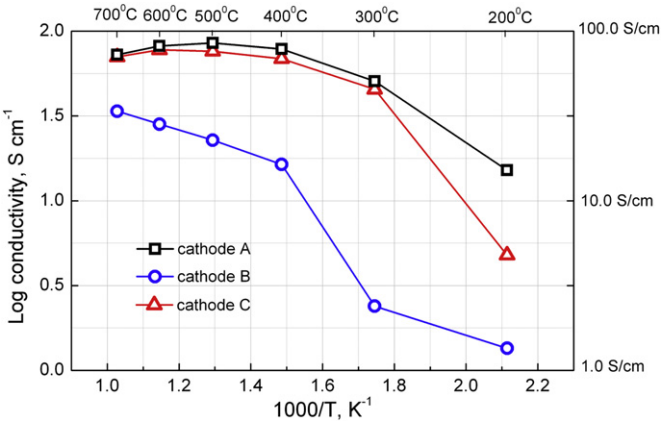

Fig. 7. Dependence of total conductivity of LSCF cells on temperature.

4. Conclusion

In summary, we successfully fabricated macroporous electrodes both in anode and cathode. This study mainly investigated the cathode, and different microstructure was compared. Using 1.5 and 0.8 μm pore former, the cathode porosity reached 42, 50%, respectively. The uniform macro pores were well distributed within cathode. At the same time, the specific surface area of cathode B and C was 28.8 and 52% larger than cathode A. As a result, the power performance improved significantly at relatively low operating temperatures (500–600 °C). For example, the peak power density of cell C was 0.25 W cm^{-2} at 550 °C, while it was just 0.11 W cm^{-2} for cell A. Thus, optimizing microstructure of cathode should be one of the approaches for lowering the operating temperature for SOFC. Furthermore, this technology allows developing new level of the cell-stack-module operable around 500 °C.

Acknowledgment

This work is supported by Japan-US clean energy technologies development.

References

[1] N.Q. Minh, J. Am. Ceram. Soc. 78 (1993) 563–588.
[2] O. Yamamoto, Electrochim. Acta 45 (2000) 2423–2435.
[3] S.C. Singhal, Solide State Ionics 152-153 (2002) 405–410.
[4] B.C.H. Steele, A. Heinzel, Nature 414 (2001) 345–352.
[5] J. Yan, H. Matsumoto, M. Enoki, T. Ishihara, Electrochem. Solid-State Lett. 8 (2005) A389–A391.
[6] Z.P. Shao, S.M. Haile, Nature 431 (2004) 170–173.
[7] S. Tao, J.T.S. Irvine, Nat. Mater. 2 (2003) 320–323.
[8] C.D. Zuo, S.W. Zha, M.L. Liu, M. Hatano, M. Uchiyama, Adv. Mater. 18 (2006) 3318–3320.
[9] E. Fabbri, L. Bi, D. Pergolesi, E. Traversa, Adv. Mater. 24 (2012) 195–208.
[10] H. Huang, M. Nakamura, P. Su, R. Fasching, Y. Saito, F.B. Prinz, J. Electrochem. Soc. 154 (2007) B20–B24.
[11] T. Suzuki, Z. Hasan, Y. Funahashi, T. Yamaguchi, Y. Fujishiro, M. Awano, Science 325 (2009) 852–855.
[12] E. Mutoro, E.J. Crumlin, M.D. Biegalski, H.M. Christen, S.H. Yang, Energy Environ. Sci. 4 (2011) 3689–3696.

[13] T. Suzuki, T. Yamaguchi, K. Hamamoto, Y. Fujishiro, M. Awano, N. Sammes, Energy Environ. Sci. 4 (2011) 940–943.
[14] M. Zhi, G. Zhou, Z. Hong, J. Wang, R. Gemmen, K. Gerdes, A. Manivannan, D. Mae, N. Wu, Energy Environ. Sci. 4 (2011) 139–144.
[15] M. Zhi, N. Mariani, R. Gemmen, K. Gerdesa, N. Wu, Energy Environ. Sci. 4 (2011) 417–420.
[16] N. Zhang, J. Li, W. Li, D. Nic, K. Sun, RSC Adv. 2 (2012) 802–804.
[17] Y. Zhang, S. Zha, M. Liu, Adv. Mater. 17 (2005) 487–491.
[18] N.M. Sammes, Y. Du, R. Bove, J. Power Sources 145 (2005) 428–434.
[19] K. Kendall, M. Palin, J. Power Sources 71 (1998) 268–270.
[20] K. Yashiro, M. Yamada, T. Kawada, J. Hong, A. Kaimai, Y. Nigara, J. Mizusaki, Electronchemistry 70 (2002) 958–960.
[21] T. Suzuki, M.H. Zahir, Y. Funahashi, T. Yamaguchi, Y. Fujishiro, M. Awano, Electronchem. Commun. 10 (2008) 1563–1566.
[22] T. Suzuki, Y. Funahashi, T. Yamaguchi, Y. Fujishiro, M. Awano, Electrochem. Solid-State Lett. 10 (2007) A177–A179.
[23] T. Suzuki, Y. Funahashi, T. Yamaguchi, Y. Fujishiro, M. Awano, J. Electronchem. Soc. 156 (2009) B318–B321.
[24] W.H. Kim, H.S. Song, J. Moon, H.W. Lee, Solid State Ionics 177 (2006) 3211–3216.
[25] L. Qiu, T. Ichikawa, A. Hirano, N. Imanishi, Y. Takeda, Solid State Ionics 158 (2003) 55–65.
[26] S.P. Jiang, Solid State Ionics 146 (2002) 1–22.
[27] B. Liang, T. Suzuki, K. Hamamoto, T. Yamaguchi, Y. Fujishiro, M. Awano, B.J. Ingram, J.D. Cater, J. Power Sources 196 (2011) 9124–9129.
[28] S.B. Adler, Solid State Ionics 111 (1998) 125–134.
[29] W. Gong, S. Gopalan, U.B. Pal, J. Power Sources 160 (2006) 305–315.
[30] K. Chen, X. Chen, Z. Lu, N. Ai, X. Huang, W. Su, Electrochem. Acta 53 (2008) 7825–7830.
[31] T. Yamaguchi, K.V. Galloway, J. Yoon, N.M. Sammes, J. Power Sources 196 (2011) 2627–2630.
[32] L.M. Ushkalov, O.D. Vasylyev, Y.G. Pryschepa, A.V. Samelyuk, V.G. Melakh, ECS Transaction 25 (2) (2009) 2421–2426.